Materials & Design 227 (2023) 111746

Contents lists available at ScienceDirect

Materials & Design

journal homepage: www.elsevier.com/locate/matdes

Data-driven thermal and percolation analyses of 3D composite structures with interface resistance

Mozhdeh Fathidoost [a,*], Yangyiwei Yang [a,*], Matthias Oechsner [b,c], Bai-Xiang Xu [a,*]

[a] Mechanics of Functional Materials Division, Institute of Materials Science, Technische Universität Darmstadt, Darmstadt 64287, Germany
[b] Institute for Materials Technology (IfW), Faculty of Mechanical Engineering, TU Darmstadt, Germany
[c] State Materials Testing Laboratory (MPA), TU Darmstadt, Germany

HIGHLIGHTS

- Importance of thermal/geometric features of composite structures to effective thermal conductivity is studied.
- Effective thermal conductivity is correlated with the features using machine learning.
- Using a machine learning model, composites are classified based on the existence of percolation path.
- Volume fraction of particles and interface thermal resistance are most influential parameters on effective thermal conductivity.

GRAPHICAL ABSTRACT

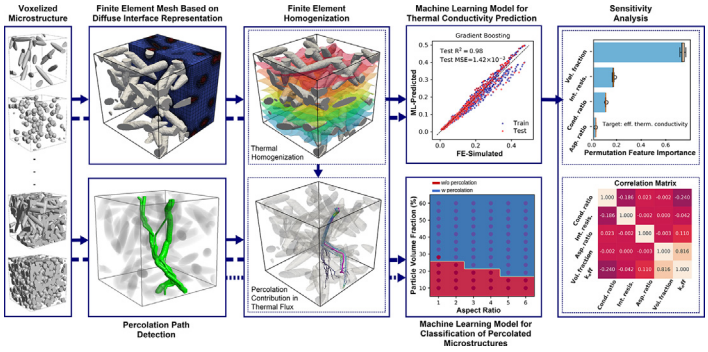

ARTICLE INFO

Article history:
Received 26 September 2022
Revised 12 February 2023
Accepted 13 February 2023
Available online 24 February 2023

Keywords:
Composite materials
3D thermal percolation
Computational homogenization
Data-driven approach
Effective thermal conductivity
Diffuse-interface
Kapitza resistance

ABSTRACT

Data-driven thermal and percolation analyses are conducted to elucidate the effects of various characteristics on the effective thermal conductivity of complex 3D composite structures. These characteristics include the thermal and geometric properties of the composite constituents, the interface resistance, and the existence of percolation paths. A series of voxel-wise microstructure samples with various characteristics are generated. Their effective thermal conductivities are evaluated using a diffuse-interface-based computational homogenization method. A voxel-based algorithm is employed to identify the potential percolation paths in the structures. The homogenization results show particularly significant effects of the percolation path in composite samples with higher aspect ratios and interface resistances. The importance of different thermal and geometric features to the effective thermal conductivity is analyzed using a data-driven sensitivity study. The analysis also demonstrates that the particle volume fraction and interface thermal resistance are the most influential characteristics for determining the effective thermal conductivity. Finally, employing a surrogate-based classification model, microstructures with and without percolation can be distinguished with an accuracy of 93%.

1. Introduction

The effective thermal conductivity (k_{eff}) of a composite structure depends on many variables, including the intrinsic characteristics of the different phases, the microstructures, and the interfaces between the different phases [1–3]. Modeling

* Corresponding authors.
E-mail addresses: mozhdeh.fathidoost@mfm.tu-darmstadt.de (M. Fathidoost), yangyiwei.yang@mfm.tu-darmstadt.de (Y. Yang), xu@mfm.tu-darmstadt.de (B.-X. Xu).

https://doi.org/10.1016/j.matdes.2023.111746
0264-1275/

approaches, including theoretical and simulation methods, are powerful tools for comprehending the effects of these factors on the k_{eff} of composites. In particular, simulation models are capable of addressing the issue for cases requiring expensive, time-consuming, and difficult-to-reproduce experimental processes [1]. Moreover, a large simulation dataset of microstructures and properties can enrich the limited experimental data and thus enable data-driven composite design [4].

The percolation paths, along with the composite constituents and interface properties, play a role in determining the transport properties of composites [5–8]. Percolation theory correlates with the formation of a truncated network in the domain, which facilitates the transition of thermal flux through long-range connectivity. Based on experimental observations [9,6], the effective thermal conductivity of composite structures increases drastically when the particle volume fraction exceeds a specific value. This is the point at which the percolation path is formed in the composite structure, which is called the percolation threshold. In other words, the enhancement of effective thermal conductivity with increasing particle content is nonlinear, based on observations from experimental and numerical studies [6,7,10,11]. Monte Carlo simulation is a well-known strategy for theoretically predicting the percolation threshold in either randomly or homogeneously distributed structures and has been widely used in previous investigations on composite structures with different pore shapes, particle shapes, and aspect ratios [10-13]. In some cases, marked enhancement of the effective thermal conductivity does not occur with an increase in the volume fraction of particles having very high thermal conductivity [14,15]. Moreover, the percolation paths are strongly influenced by the interface thermal resistance, which originates from interfacial phonon scattering in this region [16,17]. Therefore, it is important to consider both the interface thermal resistance and occurrence of percolation when calculating the effective thermal conductivity. With respect to a 3D composite structure, studies of both the percolation path and interface morphology, which are limited in the literature, become complicated.

Several analytical and numerical methods are available for predicting the effective thermal conductivities of composite materials. Analytical approaches, such as the Maxwell [18] and Bruggeman models [19], are easy to use but do not consider the details of the material distribution in a composite. By contrast, numerical approaches based on solving partial differential equations (PDE), such as the finite element method (FEM) [20], are capable of considering the morphology and distribution of particles in the composites but are very computationally expensive. With recent advances in machine learning (ML) techniques [21–23], there has been increasing interest in developing surrogate models to address engineering issues based on data analysis. ML, as a subcategory of data-driven methods, has opened a new door in the design and discovery of novel materials in the material research community. Indeed, data-driven analysis employs powerful and promising tools to unveil the implicit correlations in data, for which various ML models are available [24,25].

In general, using an ML surrogate model to predict the properties of a microstructure/composite structure has several advantages compared to the numerical simulations using physics-based mathematical models. For instance, each numerical simulation delivers effective properties of the individual structure but cannot directly provide an overarching correlation between the effective properties and the microstructure. For such purposes, a series of numerical simulations and correlation analyses are required; this is performed by ML surrogate models. In addition, soon after an ML model is trained, the prediction of effective properties for an unseen microstructure is computationally much more efficient than that using a numerical simulation. Moreover, such ML models can be easily accessed by related research communities without requiring specific numerical skills. For example, web access can be provided to a trained ML model with a graphical user interface for input and output. Furthermore, the performance and capabilities of the trained ML models can be constantly improved or expanded as they are exposed to more datasets. Thus, the models can continue to learn and recapture accumulated knowledge based on these growing datasets. Finally, ML surrogate models can be employed in combination with optimization algorithms to enable inverse design of structures.

Regarding multi-physics modeling, ML models have the potential to efficiently perform as surrogate models and support the optimization process, feature or descriptor extraction, and sensitivity analysis (SA) based on the accessible dataset [21]. To predict the effective thermal conductivity of composite materials, ML methods are classified into two types: conventional ML methods and convolutional neural networks (CNNs) [23]. CNNs are a subcategory of deep learning (DL) models. CNN models are not only capable of predicting the effective thermal conductivity but can also automatically extract the features describing the structural design of materials. Because the features extracted by a CNN are not physically understandable, conventional ML algorithms that deal with some physically intuitive features would be preferable, e.g., when the sensitivity and correlation of each physical feature to the final results should be analyzed, or when the prediction needs to be compared with some analytical approaches working on those physical features. However, it should be noted that the accuracy of conventional ML models is highly dependent on how well the features can describe the structure of the composite [26].

SA, which is another method used in data-driven analysis, quantifies the uncertainties between model parameters. SA determines the performance of an assessment by measuring the extent to which the final output is influenced, by changing the models, methods, and variable values [27–29]. Hence, SA is employed as a powerful tool to design a proposed material with the desired characteristics, as it can define the most important and dependent input variables affecting the final outcome. A sufficiently complete and large dataset is another important component of data-driven and ML techniques, and this can be obtained from either experiments or simulations.

To investigate the effective thermal conductivity of composites numerically and generate simulated data, FEM-based computational homogenization has been widely utilized [30–33]. Most of the reported FEM-based schemes for thermal homogenization of composites are based on the sharp-interface approach, which allows direct definition of the continuity conditions at the interface. However, these sharp-interface descriptions of the microstructure face both geometric and numerical challenges when handling highly complex morphologies. Thermal homogenization schemes based on the diffuse-interface description of the microstructure have thus been developed [34–37]. In these schemes, the complex geometries are recaptured by a set of continuous fields (phase indicators, as in the phase-field theory), varying between two values across an interface, and the thermal properties (mostly the thermal conductivity) are represented through the interpolation of indicators across the interface. Recently, the authors extended the diffuse-interface-based thermal homogenization to include the effects of the existing thermal (Kapitza) resistance and exceeding fluxes at the interface via anisotropic interpolation of the thermal conductivity [37].

This study aimed to investigate the influences of different thermal and geometric parameters of composite constituents, interface resistance, and percolation path on the effective thermal conductivity of composites. The importance of different characteristics to the targeted effective thermal conductivity was also investi-

gated. The other secondary goals of this study were to develop surrogate models for correlating the input parameters of the composite samples and the effective thermal conductivity response, as well as to train a model for classifying the microstructures based on the presence of a percolation path. The assessed composites consisted of a series of 3D nanocomposite structural samples with ellipsoidal particles and interfacial thermal resistance between the matrix and the particles. A previously developed diffuse-interface approach and computational finite element homogenization were adopted for the thermal homogenization and calculation of the effective thermal conductivity of the samples. A dataset consisting of composite structure descriptors was collected as the input. The effective thermal conductivity calculated by the FEM simulation and the attendant possibility of a percolation path in each microstructure constituted the output of the dataset. A sensitivity study, which is categorized as data-driven analysis, was conducted to identify the importance of different characteristics to the effective thermal conductivity. The ML models were trained as surrogate models to correlate the input parameters and the effective thermal conductivity response and to classify the microstructures with and without the percolation path.

2. Workflow and methods

The workflow and methods employed in this study are summarized as follows. First, composite structure samples were generated by a random generator using predefined characteristics (Fig. 1a_1). The digital microstructure was then employed to generate a finite element mesh with an initial sharp-interface morphology (Fig. 1a_2). Next, the microstructure with the sharp-interface was relaxed into a microstructure with a diffuse-interface (Fig. 1a_3). Subsequently, the meshed diffuse-interface microstructure was subjected to computational homogenization to estimate the k_{eff} of the corresponding geometry and thermal properties (Fig. 1b). In parallel, the voxel-wise microstructure was utilized to identify the percolation path and compared with the visualized local thermal flux from the thermal simulations (Fig. 1c). Then, SA based data-driven method was performed to analyze the contributions of different characteristics, as shown in Fig. 1d and explained in detail in Sections 2.4 and 4. Two surrogate models were trained during the analysis, one of which could map the relationship between the geometric/thermal characteristics and the corresponding k_{eff}, and the other could classify the microstructure in terms of percolation.

2.1. Generation of diverse RVEs with a diffuse-interface

To generate the representative volume elements (RVEs) of the composites, the centers of the particles in free space were distributed by employing a random value generator. Then, the dispersion of parameter-constrained particles was created in the $200 \times 200 \times 200$ voxelized domain, where a voxel value of 1 represents the particle and a voxel value of 0 represents the matrix, as shown in Fig. 1a_1. The commercial geometry generator software

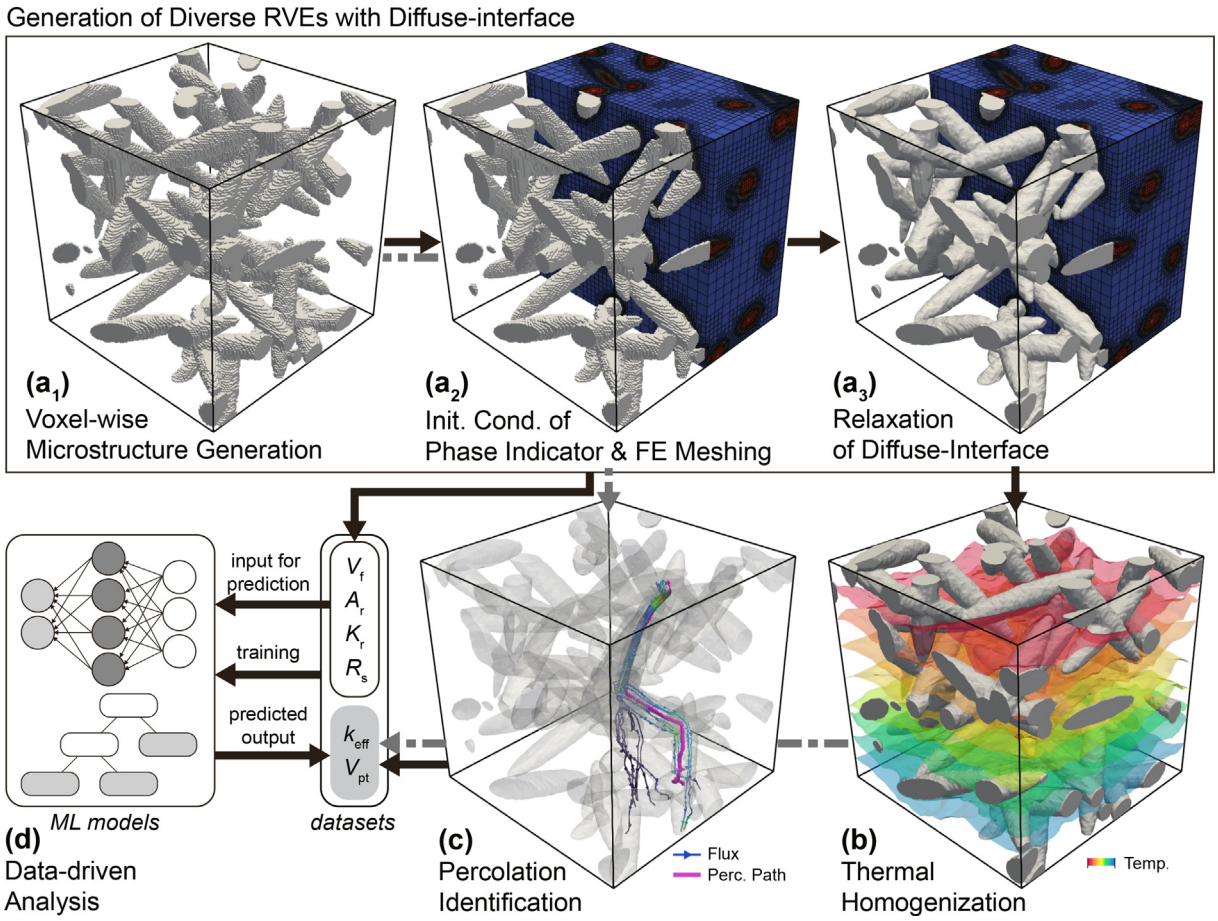

Fig. 1. Workflow of thermal percolation analysis based on the parameterized microstructure. (a_1) Generation of the voxelized microstructure; (a_2) mapping and thresholding of the initial conditions in the finite element mesh based on the generated voxels to identify the phase indicator, ϕ; (a_3) interface relaxation using the Allen–Cahn equation to obtain the diffuse-interface; (b) thermal homogenization; (c) voxel-wise identification of percolation paths; (d) data-driven sensitivity analysis of the factors affecting k_{eff} as well as surrogate-based microstructure classification in terms of including the percolation path.

GeoDict® (ver. 2021) was used to generate the parameterized microstructure.

To design the numerical experiment, this study focused on ellipsoidal particles with various geometric and thermal parameters. One of the parameterized characteristics was the aspect ratio A_r, which is defined as the ratio between the major and minor axis lengths of the ellipsoidal particles. For simplicity, all of the particles had constant minor axis lengths of 5 nm. In addition, the thermal conductivity ratio is defined as $K_r = k_{(i)}/k_{(m)}$, where $k_{(m)}$ and $k_{(i)}$ are the isotropic thermal conductivities of the matrix and the particle, respectively. The normalized Kapitza resistance, $\widetilde{R}_s = R_s k_{(i)}/l$, is another thermal characteristic of the microstructure. All of these variables and their domains are listed in Table 1. The diffuse-interface width is expressed as l.

The generated voxel-wise microstructure was then mapped into the simulation domains as the initial condition for variable ϕ, regarded as the phase indicator of the microstructure, i.e., $\phi = 1$ represents the particle and $\phi = 0$ represents the matrix (Fig. 1a_2). This process can also be extended to import a stack of images from the layer-wise characterization method, e.g., a computed tomography (CT) scan, where the pixel of each image (layer) is thresholded into binary values according to the grayscale. It is worth noting that the profile of ϕ along the normal direction across the interface must be centrally symmetric to its inflection point, e.g., a sigmoid-shaped profile in 1D. In this study, the required diffuse-interface was built by numerically applying the Allen–Cahn equation as follows:

$$\frac{\partial \phi}{\partial t} = \nabla^2 \phi - \frac{4\alpha^2}{l^2}\phi(1 - 3\phi + 2\phi^2), \tag{1}$$

where l is the nominal diffuse-interface width tuned by parameter α [38,37]. For instance, l characterizes the band $\phi \in [0.12, 0.88]$ when $\alpha = 2$, and $\phi \in [0.05, 0.95]$ when $\alpha = 2.94$. In this study, $\alpha = 2$ and $l = 1$nm were set for all microstructures. To generate a sufficient diffuse-interface without changing the morphology, each microstructure was defined using (1) for 1–3 time steps with an interval of 0.1 unit of time, as shown in Fig. 1a_3.

2.2. Computational thermal homogenization

The diffuse-interface microstructure with anisotropic interface thermal conductivity was numerically verified in [37] with an analytical temperature profile and closed-form thermal homogenization models (e.g., the Maxwell estimation based on the microstructure with sufficiently distanced spherical particles). For the sake of completeness, a summary of the model and its formulations is given below. As discussed in [37], the phase-dependent local conductivity tensor, $\mathbf{k}$, must be formulated anisotropically with distinct eigen-conductivities, $k_\perp$ and $k_\parallel$, between the normal and tangent directions of the diffuse-interface, respectively.

$$\mathbf{k}(\phi) = k_\perp(\phi)\hat{\mathbf{n}} \otimes \hat{\mathbf{n}} + k_\parallel(\phi)(\mathbf{I} - \hat{\mathbf{n}} \otimes \hat{\mathbf{n}}), \tag{2}$$

where the normal vector, $\hat{\mathbf{n}}$, is represented by the gradient of the phase indicator, ϕ, i.e., $\hat{\mathbf{n}} = \nabla\phi/|\nabla\phi|$; $\mathbf{I}$ is the identity tensor; and $\Phi_{(i)}$ and $\Phi_{(m)}$ are interpolation functions that are equal to one and zero in the particle and matrix, respectively. To guarantee continuity conditions along the normal and tangent directions (explained in Supplementary Note 1 of Ref. [37]), the phase (ϕ)-dependent interpolations in $k_\parallel$ and $k_\perp$ are formulated as follows:

$$\begin{aligned} k_\parallel(\phi) &= k_{(i)}\Phi_{(i)}(\phi) + k_{(m)}\Phi_{(m)}(\phi), \\ k_\perp(\phi) &= \frac{k_{(i)}k_{(m)}}{k_{(m)}\Phi_{(i)}(\phi) + k_{(i)}\Phi_{(m)}(\phi) + k_{(i)}k_{(m)}R_s|\nabla\phi|}. \end{aligned} \tag{3}$$

In this study, diffuse-interface-based computational thermal homogenizations were performed to evaluate the k_{eff} of the geometrically complex microstructure based on our recent work [37]. The governing equations are Fourier's law and the conservation law:

$$\begin{cases} \mathbf{j} &= -\mathbf{k} \cdot \nabla T, \\ \nabla \cdot \mathbf{j} &= 0, \end{cases} \tag{4}$$

where T is the temperature field, $\mathbf{j}$ is the thermal flux, and $\mathbf{k}$ is the defined local conductivity. The thermal homogenization problem can then be defined as follows:

$$\begin{cases} \mathbf{j} &= \mathbf{k}(\phi) \cdot \nabla T \quad \text{on microscale}, & (5) \\ \langle \mathbf{j} \rangle &= \mathbf{k}_{\text{eff}} \cdot \langle \nabla T \rangle \quad \text{on macroscale}, & (6) \end{cases}$$

where $\mathbf{k}_{\text{eff}}$ is the homogenized effective thermal conductivity tensor with an effective value $k_{\text{eff}} = \text{tr}(\mathbf{k}_{\text{eff}})/3$, which is evaluated in this study; $\langle\cdot\rangle = \int_\Omega(\cdot)\text{d}\Omega/\Omega$ is the mean operator. Note that the Hill-Mandel condition for the thermal conduction problem should be satisfied as follows:

$$-\langle \mathbf{j} \cdot \nabla T \rangle = -\langle \mathbf{j} \rangle \cdot \langle \nabla T \rangle = \langle \mathbf{j} \rangle \cdot \langle -\nabla T \rangle. \tag{7}$$

This condition implies that the thermal dissipation at the microscale should be equal to that at the macroscale. To satisfy the Hill-Mandel condition, a linear temperature boundary condition is employed:

$$T|_\Gamma = \mathbf{g} \cdot \hat{\mathbf{x}}, \tag{8}$$

where the prescribed constant temperature gradients, $\mathbf{g}$, represent the macroscopic effect, and the coordinates $\hat{\mathbf{x}}$ indicate the domain boundary, $\Gamma = \partial\Omega$. Thus, the mean temperature gradient was calculated as $\langle \nabla T \rangle = \mathbf{g}$, while $\langle \mathbf{j} \rangle$ was evaluated via solving the thermal conduction problem (shown in Eq. (5)) at the microscale. Eventually, the component k_{ij}^{eff} of the homogenized thermal conductivity tensor was evaluated by calculating three components $\langle j_i \rangle$ under three separately imposed gradients, g_j, parallel to the corresponding axis, i.e., i and $j = x, y, z$, as follows:

$$k_{ij}^{\text{eff}} = \langle j_i \rangle / g_j. \tag{9}$$

The models were numerically implemented by FEM in the simulator NIsoS, which was developed by the authors based on the MOOSE framework [39,40]. Eight-node hexahedral Lagrangian elements were used to mesh the geometry. A nonlinear solver with the preconditioned Jacobian-free Newton–Krylov method (PJFNK) was employed for both diffuse-interface generation and the computational thermal homogenization calculations. The time differential in the transient problem was calculated using the backward Euler method. The large-scale parallel CPU computations for each simulation case, which had degrees of freedom on the order of 10,000,000 for both nonlinear and auxiliary systems, were performed with 96 processors and 10 GByte RAM per processor. Each simulation consumed eight core-hour on average.

Table 1
Geometric and thermal parameters employed in the generated microstructures.

Parameters	Value (Unit)	Type	Increment
Minor principal axis length	5 (nm)	Constant	–
Aspect ratio, A_r	$[1, 6]$	Linear	1
Particle volume fraction, V_f	$[5, 60]$	Linear	5
Thermal conductivity ratio, K_r	$[15, 100]$	Linear	15
Normalized interface resistance, $\widetilde{R}_s$	$\left[10^{-6}, 10^{10}\right]$	Logarithmic	10^2

2.3. Percolation identification

In the digital voxel-wise microstructure, a pathway composed of particles that starts from one side of the RVE and ends on the other side is regarded as a percolation path. In this study, an algorithm was employed to identify percolation paths with denoted starting and ending sides.

When several paths from beginning to end are fully attached, the algorithm considers them as only one path with a specific cross-sectional diameter. It should be noted that voxels connected only via the corners were not considered as connected phases. In this regard, the voxels should have at least one common face. Finally, the coordinates of the voxel centers lying in the middle of the percolation path were extracted to construct the analytical percolation path.

2.4. Data-driven thermal analysis

Data-driven thermal analysis was performed to extract meaningful knowledge from a dataset obtained from batched computational homogenizations and percolation identification. In this study, two objectives were pursued using data-driven analysis. One was to identify the most important thermal or geometric characteristics of the composite microstructure that were significant to k_{eff}; the other was to identify whether a composite microstructure contained a percolated phase based on the geometric characteristics. In addition, the tree diagram in Fig. 2a presents the objectives of the data-driven analysis and the corresponding methods to achieve these goals. Based on these two targets, the workflow of the data-driven analysis also consisted of two main parallel streams. For the first stream, two methods for SA were employed: permutation feature importance and Pearson coefficient analysis. The surrogate model required for permutation feature importance

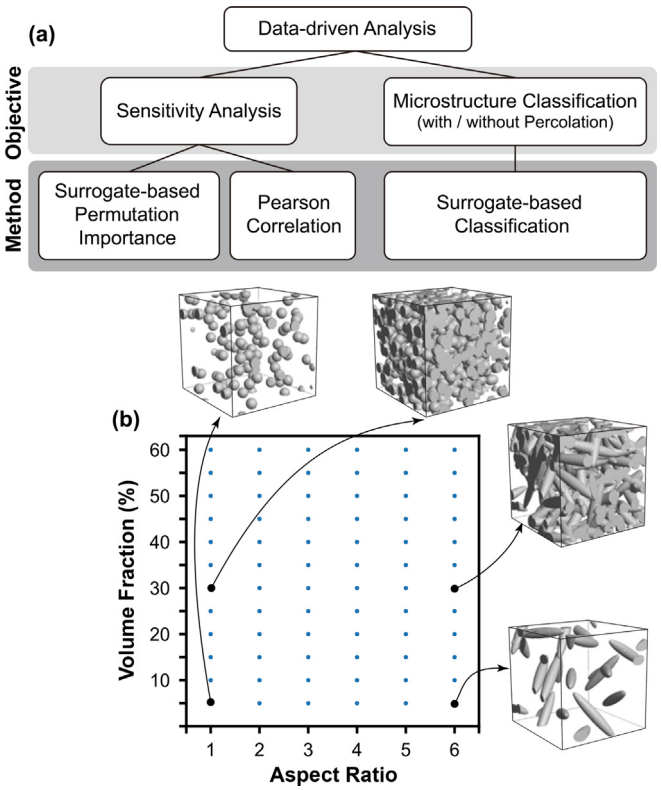

Fig. 2. (a) Tree diagram representing the data-driven analysis; (b) illustration of selected geometries in the dataset for the data-driven analysis.

was developed using an ML model. It was trained on the input data, including thermal and geometric features describing the materials, and the output data included the FEM simulation results. A classification surrogate model was built that targeted the second workflow stream. The model was trained using the geometric features of the simulated composites as the input and the result of a voxel-wise percolation identification algorithm for the presence of a percolation path in the composite as the output. Each step is clarified in more detail below.

SA is used to determine the correlation between the variations in the output and the different sources of variations within the assumptions, i.e., the dependence of the composite k_{eff} on the geometric design and thermal parameters.

In the first approach to SA, the Pearson correlation, $R_{\mathbf{X},\mathbf{Y}}$, given by (10), was used to define the importance of the characteristics, where $\mathbf{X} = [x_1, x_2, \ldots, x_i]$ and $\mathbf{Y} = [y_1, y_2, \ldots, y_i]$ are the input and output vectors, respectively, $\text{cov}(\cdot)$ is the covariance operator, and $\sigma_{\mathbf{X}}$ and $\sigma_{\mathbf{Y}}$ are the standard deviations of $\mathbf{X}$ and $\mathbf{Y}$, respectively. A perfect negative linear correlation between the two variables is represented by a value of -1. A value of 0 indicates that there is no linear correlation between the two variables. A completely positive linear correlation between the two variables is indicated by a value of 1. The stronger the correlation between the two variables, the further from zero the correlation coefficient will be.

$$R_{\mathbf{X},\mathbf{Y}} = \frac{\text{cov}(\mathbf{X},\mathbf{Y})}{\sigma_{\mathbf{X}}\sigma_{\mathbf{Y}}}. \tag{10}$$

The permutation importance methodology was also used for SA, where the importance of a characteristic is calculated by measuring the increase in the prediction error of the model after permuting a feature to determine its relevance. Because the prediction of a model relies on the input characteristics, an important feature is the one that increases the prediction model error after permutation. However, a characteristic is less important when altering its values does not affect the model error. Therefore, this characteristic is negligible for prediction in this case.

The prerequisite for permutation importance is building a model to predict the desired output based on the present input characteristics, e.g., employing ML. Depending on the tasks at hand, different ML models are available. In the present case, a regression problem was considered to map the thermal/geometric parameters to the k_{eff} of the composite structures. Widely used models are available for such problems, like support vector regression (SVR) [23,26]. These are well implemented and available in Scikit-learn, an ML library for Python [41]. In this study, different ML algorithms were used as surrogate models for performing SA using the permutation approach. The first algorithm was the K-nearest neighbors (KNN), which is a nonparametric supervised learning algorithm. In KNN, the output is calculated as the average of K closest neighbor values because it assumes that adjacent data points are similar. The other algorithm used was a multilayer perceptron (MLP), which is a model for nonlinear mapping between an input and output vector; the model is composed of a network of linked neurons [42]. Gradient boosting (GB), which is an ensemble technique, was also used. GB combines numerous weak models to achieve better overall performance. Decision tree (DT) is another algorithm used in this study; DT is based on the separation of data into branches of potential output, and a random forest (RF) is an ensemble model of several DTs. The final algorithm used in this study was SVR, which seeks to match the best mapping within a threshold value. This is in contrast to other regression models that aim to reduce the error between the real and predicted values. More details regarding the ML algorithms can be found in [43]. However, regression models require features to be selected for the considered problem. The selection of features that can describe

a material system is an essential step in ML. Therefore, the dataset including the selected geometric and thermal features was curated carefully. Geometric features, i.e., the particle volume fraction and aspect ratio, have been reported to be important features for the thermal conductivity of composites [26,23]. The other thermal features included were K_r and R_s.

To test the performance of the surrogate models with the aforementioned algorithms, R-squared (R^2) and mean squared error (MSE) were used, as presented in Eqs. (11) and (12), respectively; where $N, \hat{y}, \bar{y}$, and y_n are the total number of samples, predicted value, mean value of the output in the dataset, and real value, respectively. Models with R-squared values closer to 1 and smaller MSE values can be categorized as having better performance. It should be noted that for all algorithms, the default settings were used.

$$R^2 = 1 - \frac{\sum_{n=1}^{N}(y_n - \hat{y})^2}{\sum_{n=1}^{N}(y_n - \bar{y})^2}, \tag{11}$$

$$\mathrm{MSE} = 1/N\sum_{n=1}^{N}(y_n - \hat{y}_n)^2. \tag{12}$$

The dataset contained approximately 2900 computational thermal homogenization records of different composite structures with different geometric/thermal parameters, i.e., V_f, A_r, R_s, and K_r. Table 1 presents the total thermal and geometric parameters, which provided the large dataset needed for this study. To better understand the geometric vastness of the dataset, some RVEs from the dataset are illustrated in Fig. 2b. The blue points represent 72 microstructures in the dataset. The corresponding microstructures of some points are visualized as examples. It should be noted that Fig. 2b shows only the variation in the dataset in terms of geometric features.

ML-based surrogate models were trained and subsequent data-driven analyses were performed using the Scikit-learn package [41], coded in Python (ver. 3.8.8) on a PC with a 2.5 GHz Intel core i5-7200 processor and 8 GB of RAM. The training process is explained in more detail in Section 4.

3. Results and discussion

Focusing on the relative characteristics of the percolated structures, the resulting quantities presented hereafter adopt normalized forms. In this study, the thermal conductivity of particle $k_{(i)}$ was taken as the reference thermal property, together with the reference length $\bar{l} = 1$ nm and temperature $\bar{T} = 1$ K. In other words, for a given $k_{(i)}$, the normalized thermal resistance is $\tilde{R}_s = R_s\bar{l}/k_{(i)}$, and the normalized thermal flux is $\tilde{j} = jl/k_{(i)}\bar{T}$.

3.1. Convergence test on the RVE size

Choosing an appropriate size for the RVE is essential for evaluating the thermal properties (i.e., k_{eff}) of the composites. The RVE should be as small as possible to reduce the computational cost. However, the RVE should be sufficiently large to represent the microstructure of the material system accurately [44–46]. Thus, a convergence test concerning the k_{eff} for various RVE edge lengths (i.e., 25–150 nm) was performed [47]. Here, only RVEs with particles having the largest aspect ratio, i.e., $A_r = 6$, were tested because if k_{eff} exhibits a decent convergence in this case, then it will be sufficient for other cases, i.e., particles with smaller A_r. The convergence tests with $A_r = 6$ were also performed for both $V_f = 5\%$ and 60%, forming the lower and upper bounds, as collectively demonstrated in Fig. 3. For all test cases, $\tilde{R}_s$ and K_r were defined as 10^{-4} and 10, respectively.

To reduce the potential effects of randomness, notably, the randomness introduced by microstructure random generator, three distinct microstructures with different random seeds were generated for each RVE size. The calculated k_{eff} of these RVEs are shown in Fig. 3. The red line with cross markers and the blue line with dot markers represent the k_{eff} values of RVEs with different edge sizes for V_f of 5% and 60%, respectively. The Green and orange areas around the lines represent the uncertainty error in the k_{eff} measurements for three randomly generated RVEs with different random seed numbers. It can be seen that the k_{eff} values for RVEs with edge lengths greater than 100 nm exhibited a clear trend of convergence. Therefore, it can be concluded that an RVE size of 100 × 100 × 100 nm can sufficiently and properly represent the microstructure of the composites.

3.2. Demonstration of percolation paths in the simulation results

Percolation generally occurs when the particle V_f is sufficiently large. Herein, the contribution of existing percolation paths to the enhancement of k_{eff} is demonstrated. Because visualization of the percolation path is easier for higher A_r, the microstructure with $A_r = 6$ is selected as an example. K_r and $\tilde{R}_s$ in this case were both set to 100. Fig. 4a presents the homogenized k_{eff} for RVEs with V_f ranging from 5% to 60%. The point at which the curve changes its condition from linear to nonlinear is the percolation threshold, which is estimated as $V_f = 15\%$ here.

The voxel-wise algorithm for percolation identification (Section 2.3) was also executed on the microstructure with $V_f = 15\%$, as visualized in Fig. 4b. The resulting analytical percolation path is indicated by the purple line in Fig. 4c. The colors and sizes of the arrows represent the magnitude of the thermal flux. It is clear that the filtered volume with enhanced thermal conduction agreed with the geometric percolation path identified by the voxel-wise algorithm. Based on the visualized simulation results, the enhancement of local thermal conduction can be attributed to the formation of the percolation path. Consequently, a nonlinear increase in the overall k_{eff} is observed after exceeding the percolation threshold of the composite.

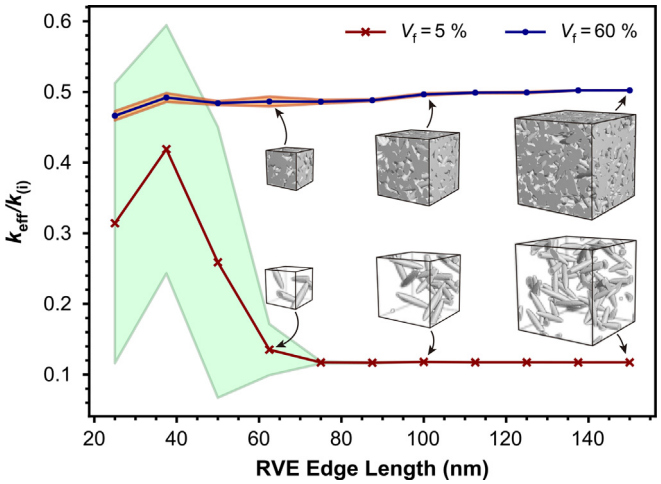

Fig. 3. RVE convergence tests for various RVE edge lengths (25–150 nm) for microstructures with $A_r = 6$. The red curve represents $V_f = 5\%$ and the blue curve represents $V_f = 60\%$.

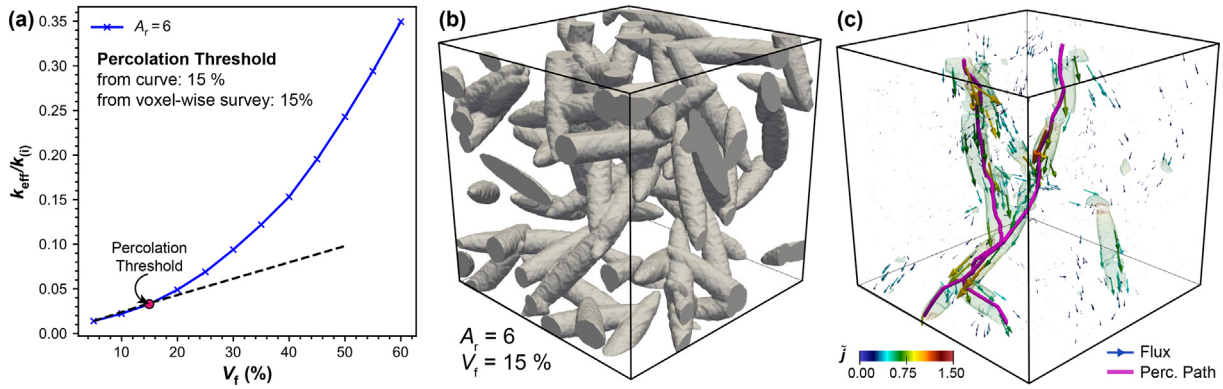

Fig. 4. (a) Results of the thermal homogenization of different RVEs with defined parameters of $A_r = 6, V_f = 5\% - 60\%, K_r = 10^2$, and $\widetilde{R}_s = 10^2$. (b) Structure of the RVE at the percolation threshold, i.e., $V_f = 15\%$. (c) The filtered volume with enhanced thermal conduction is in agreement with the geometric percolation path (purple line). The size and colors of the arrows also show the magnitude of thermal flux in the whole structure.

3.3. Impacts of various parameters

3.3.1. Particle aspect ratio

In this section, the effect of the aspect ratio on the percolation threshold is discussed. A 3D plot of k_{eff} vs. A_r vs. V_f is shown in Fig. 5a. For all cases, K_r and $\widetilde{R}_s$ were set to 10 and 10^{-4}, respectively. For a better comparison, all of the results for various k_{eff} were normalized to the values of k_{eff} with identical V_f and $A_r = 1$. The results show that for V_f in the range of 20–35%, a higher A_r causes a major increase in k_{eff} by increasing V_f. This range is where the formation of a percolation path is expected. Therefore, the drastic increase in k_{eff} can be attributed to the formation of percolation. In other words, it is supposed that in V_f smaller than the mentioned range, percolation paths are not formed, whereas in V_f larger than this range, the microstructure is saturated with percolation paths, and such a large change in k_{eff} is no longer seen.

The existence of the percolation path among the generated RVEs with equal A_r was investigated by employing the voxel-wise percolation identification algorithm described in Section 2.3. The investigation began with the smallest V_f, i.e., $V_f = 5\%$. Then, the V_f of the first microstructure showing a percolation path was reported as the percolation threshold for each individual A_r. The percolation paths at the percolation thresholds for RVEs with different A_r values are shown in Fig. 5b. The results show that for RVEs with a higher aspect ratio, the percolation threshold occurred at a lower V_f. For some A_r, e.g., $A_r = 3$ and 4, it can be observed that their percolation thresholds were the same, i.e., at $V_f = 20\%$. Because the prescribed V_f parameters used to generate composite structures in this study have discrete values between 5% and 60% with an increment of 5%, the reported percolation thresholds in terms of V_f have a tolerance of 5%. However, percolation formation can be initiated in structures with V_f that do not appear in the dataset. This can be further verified in Fig. 5b, where the amount of percolation paths identified at higher A_r for the same V_f is greater; alternatively, in terms of the visualized size, it is thicker than the percolation path at lower A_r with the same volume fraction, implying the existence of a percolation threshold between defined particle volume fractions in the dataset.

3.3.2. Interface thermal resistance

The interface thermal resistance between the particle and matrix is denoted by $\widetilde{R}_s$. The effect of $\widetilde{R}_s$ on k_{eff} over the entire range of V_f for $A_r = 1$ and 6 and $K_r = 10$ is shown in Fig. 6a. It can be observed that the results obtained for both A_r values show the same trend. For lower $\widetilde{R}_s$, i.e., $\widetilde{R}_s < 10^2$, an increase in V_f causes a greater increase in k_{eff}. Consequently, all of the curves for different $\widetilde{R}_s$ diverge at higher V_f. In addition, the curves for lower $\widetilde{R}_s$ have a more linear shape, which means that the relationship between k_{eff} and V_f is more directly linear. By contrast, for higher $\widetilde{R}_s$, i.e., $\widetilde{R}_s > 10^4$, k_{eff} increases drastically at a certain V_f, and the shapes of the curves are closer to exponential forms, which is characteris-

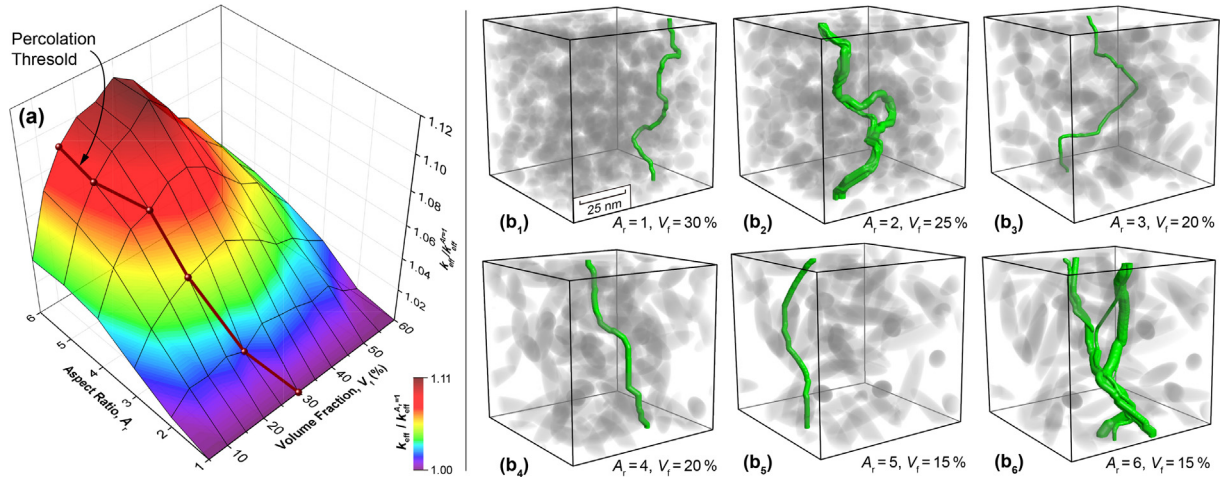

Fig. 5. (a) 3D plot of $k_{eff}/k_{eff}^{A_r=1}$ vs. A_r and V_f, (b) analytical percolation path (green line) and percolation threshold in terms of V_f for different geometries.

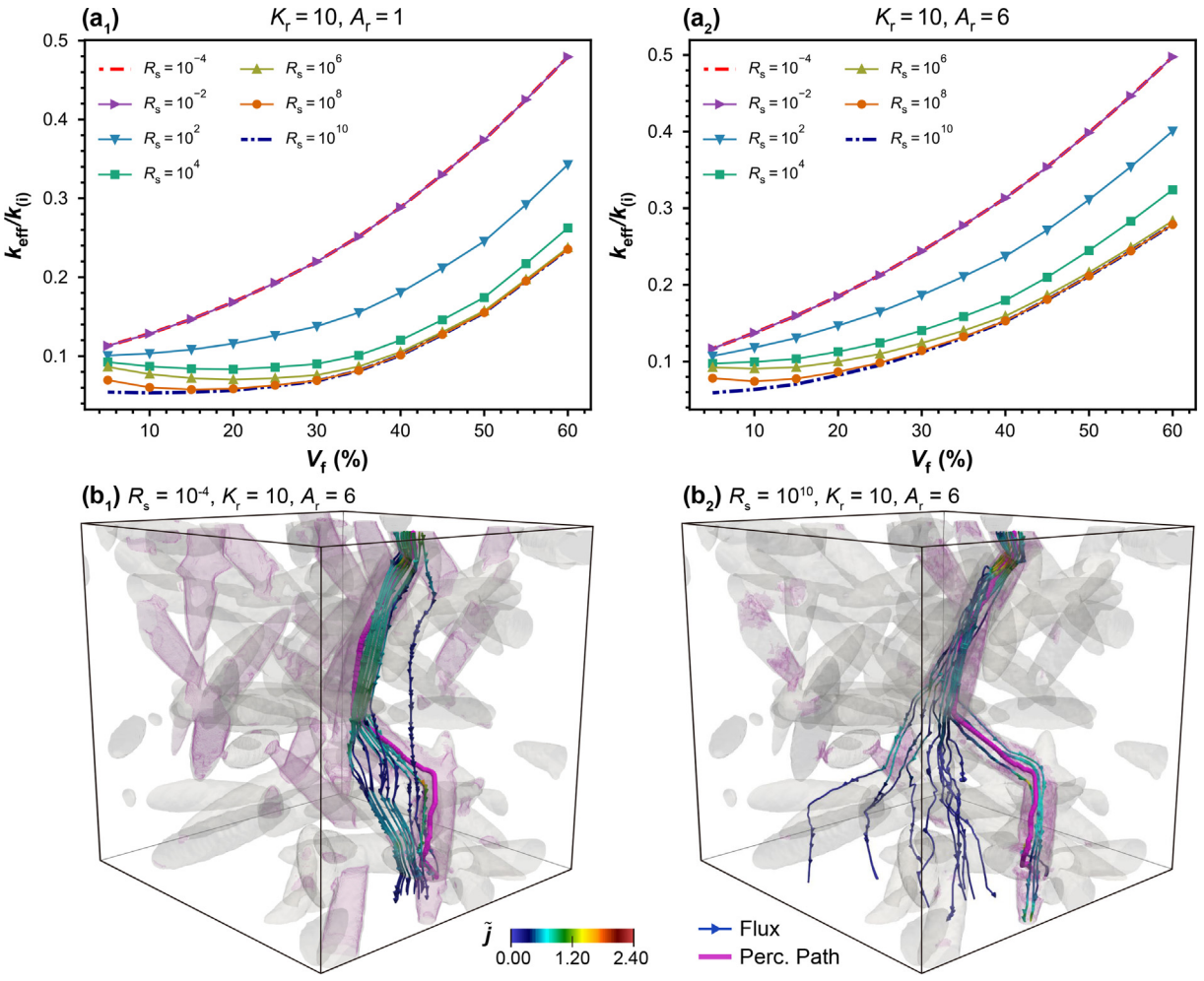

Fig. 6. Effect of $\widetilde{R}_s$ on k_{eff} with increasing volume fraction for $K_r = 10$ and $(a_1)\, A_r = 1$ and $(a_2)\, A_r = 6$. Thermal fluxes in different RVEs with $K_r = 10, A_r = 6, V_f = 15\%$, and (b_1) $\widetilde{R}_s = 10^{-4}$ and (b_2) $\widetilde{R}_s = 10^{10}$.

tic of percolation path formation. These observations imply that the main method for thermal flux is limited to the geometric percolation path for composites with high $\widetilde{R}_s$ values. To verify this claim, the thermal flux in the RVEs is shown in Fig. 6b for interface resistances $\widetilde{R}_s = 10^{-4}$ and 10^{10}. The other parameters for these geometries consist of $K_r = 10, V_f = 15\%$, and $A_r = 6$. Here, the gray regions represent the whole particles in the RVE, and the purple volumes depict regions with a high thermal flux of greater than 0.5. In addition, the thermal flux arrows and percolation path are represented by the arrows and solid purple lines, respectively. The presented thermal fluxes are limited to those originating from a sphere on the top side of the RVE, near the point where the percolation path begins. For low $\widetilde{R}_s$ (Fig. $6b_1$), the flux preferentially flows along straight paths, regardless of the orientation and location of the particles and percolation path. However, at higher $\widetilde{R}_s$ (Fig. $6b_2$), the thermal flux preferentially selects longer pathways along the percolation path to avoid the high resistance at the interface, rather than traversing shorter and straighter paths. For the thermal fluxes that leave the percolation path, returning to the percolation path is difficult. This is because they must pass through the high-resistance interface region. Consequently, these fluxes experience high scattering in the microstructure. Therefore, k_{eff} in composites with high $\widetilde{R}_s$ is mainly influenced by the formation of the percolation path and reaching the percolation threshold.

3.3.3. Thermal conductivity ratio of the particle and matrix

The other study considered is the effect of K_r on k_{eff} of the composite for different V_f values. The results of the investigation for $K_r = 15, 25, 40, 55, 70,$ and 100; $A_r = 1$ and 6; and $\widetilde{R}_s = 10^4$ are shown in Fig. 7a. For better comparison, all of the results for different K_r values were normalized to the values of k_{eff} for $K_r = 10$. With respect to the observations, a larger K_r leads to a higher increase in the thermal conductivity by increasing the volume fraction. Consequently, a larger contribution of the percolation path to the heat transfer is expected.

In this study, K_r was investigated in the range of 10–100, which is the typical range of thermal conductivity for high-temperature nanocomposite material, e.g., polymer-derived ceramics [48]. In addition, the present model only considers the heat conduction between adjacent phases, without considering the existence of highly thermally resistant cavities. Furthermore, the temperature distribution computed by this diffuse-interface model was validated successfully with theoretical models such as the Maxwell model for K_r of up to 100 in our previous study [37]. Nevertheless, in a few studies, models capable of thermal homogenization at higher K_r are reported (for instance in [49,9]), which is not the aim of this study. For better clarity, the thermal flux along the percolation line for $K_r = 10$ and 100 is shown in Fig. 7b. As expected, the flux in the RVE with higher K_r prefers the percolation phase as the best path with less hindrance to flow. This means that the percolation phases are critical in this situation.

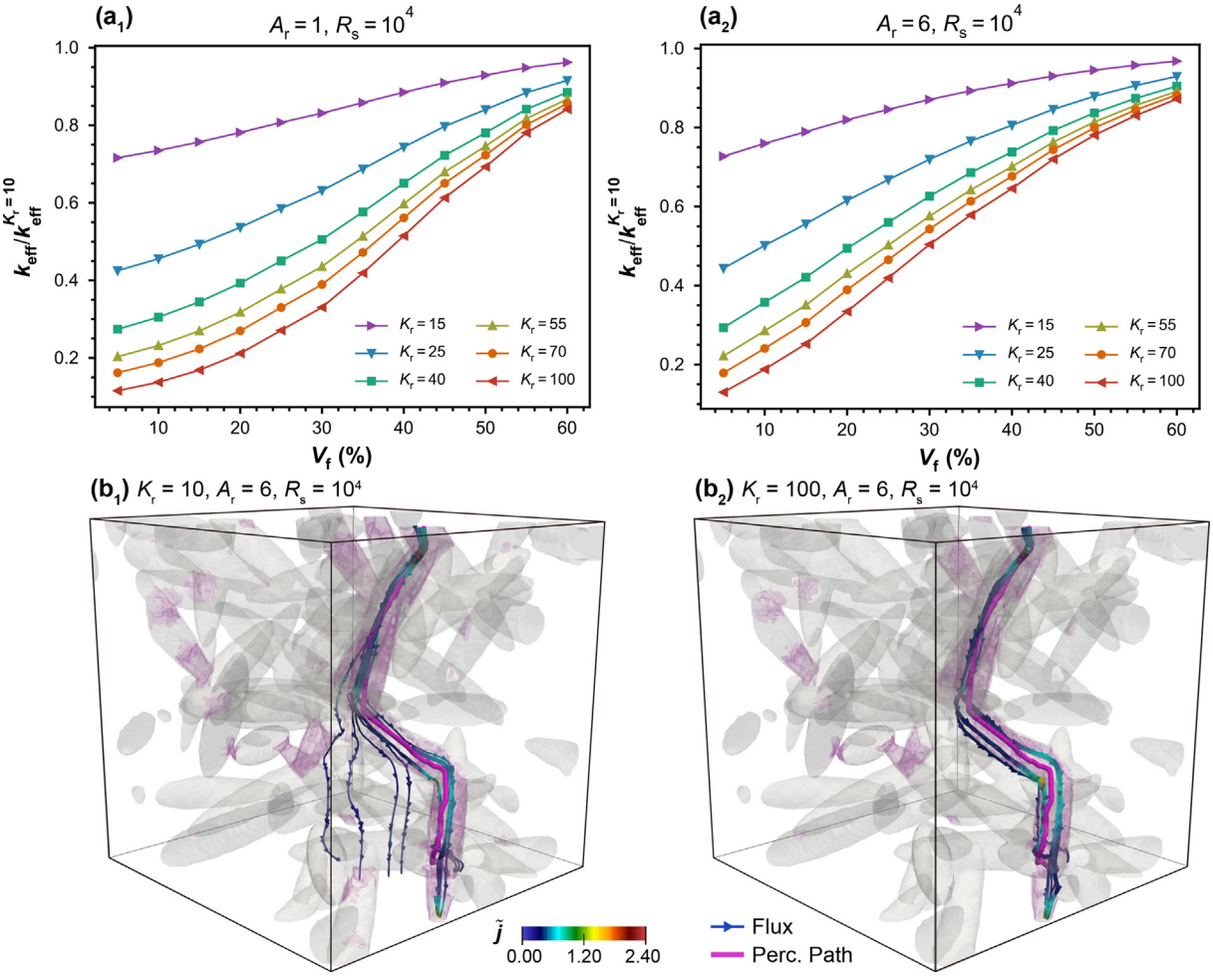

Fig. 7. Effect of K_r on k_{eff} with increasing volume fraction for $\tilde{R}_s = 10^4$ and (a_1) $A_r = 1$ and (a_2) $A_r = 6$. Thermal fluxes in different RVEs with $A_r = 6, \tilde{R}_s = 10^4, V_f = 15\%$, and (b_1) $K_r = 10$ and (b_2) $K_r = 100$.

4. Results of the data-driven analysis

To elucidate the importance of different thermal and geometric characteristics and the correlation between these parameters and the final k_{eff}, two different approaches were used: the Pearson correlation matrix and permutation importance. In the permutation method, the importance of characteristics is measured by quantifying their importance for specific models. Therefore, establishing a model is a prerequisite for this technique. Accordingly, six different ML algorithms, as described in Section 2.4, were utilized to establish surrogate models to correlate k_{eff} as the output with the input characteristics, i.e., $V_f, K_r, \tilde{R}_s$, and A_r. Based on the feature selection step described in Section 2.4, all of the utilized models were trained on the dataset, using 80% and 20% of the entire dataset for training and testing, respectively. The training process lasted for a few seconds owing to well-described features, sufficient amount of training data, and simple data structure, which can be seen as a matrix consisting of real-valued numbers. When ML models are trained, it is essential to evaluate their predictive performance before using them in the permutation because the performance of the used model needs to be accurate in this method. A comparison of the ML models and their predictive performance in terms of MSE and R^2 is shown in Fig. 8. Based on the evaluation, GB had the best performance with $MSE = 1.42 \times 10^{-3}$ and $R^2 = 0.98$. As the model results already demonstrated very promising $R^2 = 0.98$ for the GB model, the hyperparameter tuning step could be avoided.

The SA analysis based on permutation importance using GB as the surrogate model is shown in Fig. 9a. The V_f of particles is the most influential characteristic in defining k_{eff}, followed successively by $\tilde{R}_s, K_r$, and A_r. The SA results obtained using correlation matrix method are shown in Fig. 9b. The absolute value of the correlation coefficient between k_{eff} and V_f is closest to 1. This means that the Pearson correlation also recognizes V_f as the most important characteristic in defining k_{eff}, followed by K_r, A_r, and finally $\tilde{R}_s$.

From a statistical perspective, it should be noted that the Pearson matrix can only consider the linear relationship between characteristics. From a physical perspective, regarding [16], the interface density (interfacial area per unit volume) is primarily responsible for k_{eff} in nanocomposites. Therefore, $\tilde{R}_s$ has a major impact on the k_{eff} of fine-structured composites. In addition, the percolation paths formed by these fine particles are narrow and, consequently, less effective in improving the thermal conductivity of random nanocomposites over a wide range of V_f. Based on these justifications, the results obtained from the permutation importance are more valid. After V_f, this method considers $\tilde{R}_s$ as the most important characteristic for controlling the k_{eff} of composites.

Moreover, the DT algorithm was used in the surrogate-based classification method to distinguish microstructures with and without percolated particles. To this end, all of the microstructure

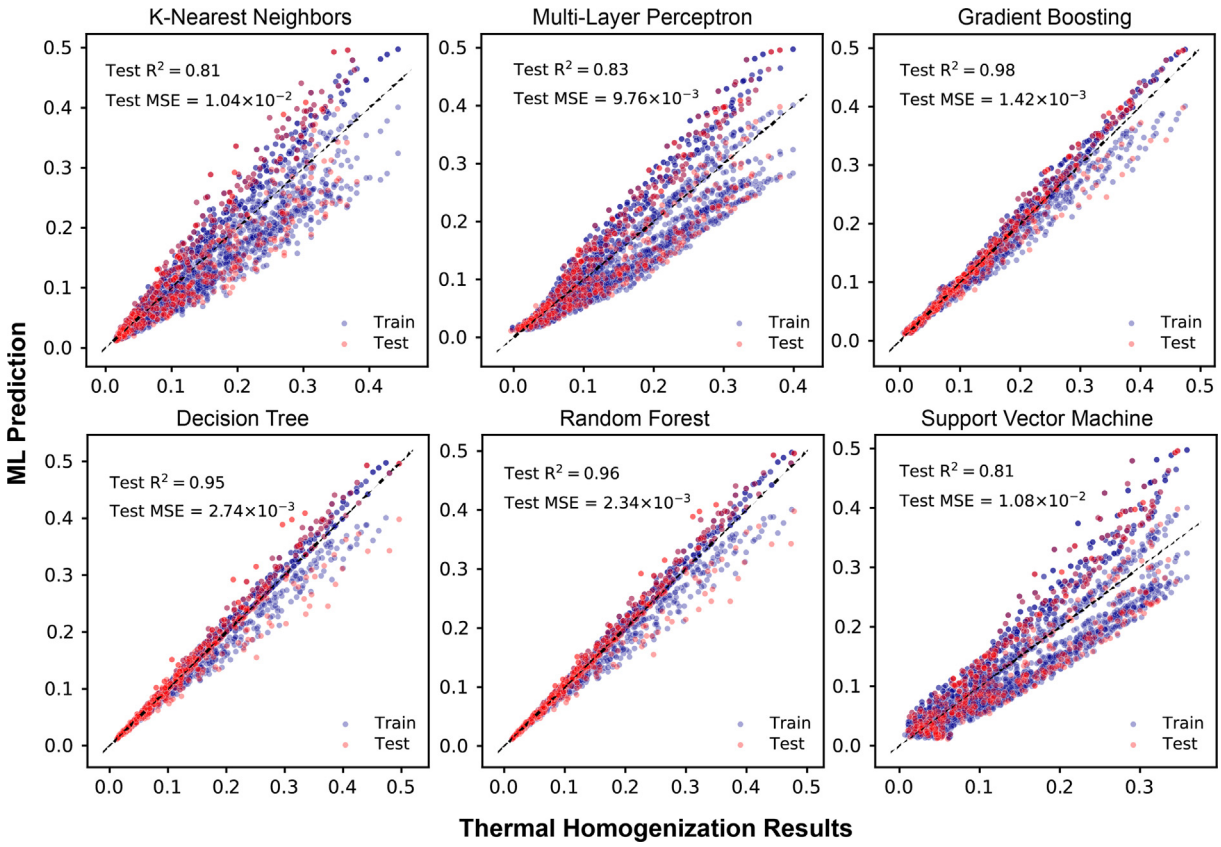

Fig. 8. Scatter plots of k_{eff} values predicted by ML models versus the simulated results obtained through thermal homogenization.

samples in the dataset were prechecked with the voxelized algorithm described in Section 2.3 to determine whether they contained a percolation path. The geometric characteristics of the microstructures consisting of V_f and A_r were used as the input of the model. Whether the microstructure was percolated was the output of the model. It means that the output of the model was Boolean type, i.e., 1 for percolated microstructure and 0 for microstructures without percolation. Next, the ML model was trained using the training data. The hyperparameter settings for the DT algorithm were the same as the default settings in the Scikit-learn package. The model achieved an R^2 of 0.93 and MSE of 0.066 for the unseen new data. The classification results are visualized in Fig. 9c. The dark blue and red dots represent the samples with and without percolation, respectively. The classification result of the ML model is illustrated by two different regions with different colors (red and blue). If the corresponding data point of a test case is located in a red area, it is assumed to be a nonpercolated microstructure. However, if it is located in a blue area, the relevant microstructure corresponding to the data point contains a percolation path. The narrow yellow line between these areas indicates the percolation threshold. The results show that the model can correctly predict the presence of the percolated phase, except for one data point with $V_f = 30\%$ and $A_r = 1$. It is expected that increasing the size of the dataset will improve the performance of the model.

This study showed that two characteristics, V_f and A_r, mostly determine the possibility of a percolation path. Nevertheless, as a methodology study, it was shown that an ML-based classification surrogate model could distinguish composite microstructure samples based on the presence of a percolation path, which can potentially be extended to more complex microstructures with several phases and multiple geometric descriptors.

5. Conclusion

A comprehensive 3D study of the thermal properties of composites with ellipsoidal particles was conducted using FEM-based computational thermal homogenization and data-driven approaches. The diffuse-interface model was used to interpret the composite structure because it has the advantage of overcoming challenges related to complex microstructures. The geometric percolation path formed within the composite structure was also explored. Subsequently, its contribution to the leading thermal flux inside the material was qualitatively investigated. In addition, six different ML algorithms were used to develop surrogate models. The models were then used to predict the effective thermal conductivity based on the thermal and geometric characteristics of RVEs. The GB algorithm outperformed the other models, with an R^2 of 0.98. Based on the developed ML model, a data-driven SA was used to determine the importance of different composite characteristics to the effective thermal conductivity of the composite, i.e., $A_r, V_f, \tilde{R}_s$, and K_r. The results obtained from the simulation and data-driven analysis are summarized below:

(i)The heat flux along the percolation path in a 3D microstructure was qualitatively studied and visualized using the FEM simulation results of thermal homogenization. The thermal flux preferentially flows along the percolation path, particularly for larger values of the interface thermal resistance and thermal conductivity ratio. In these cases, the formation of a percolation

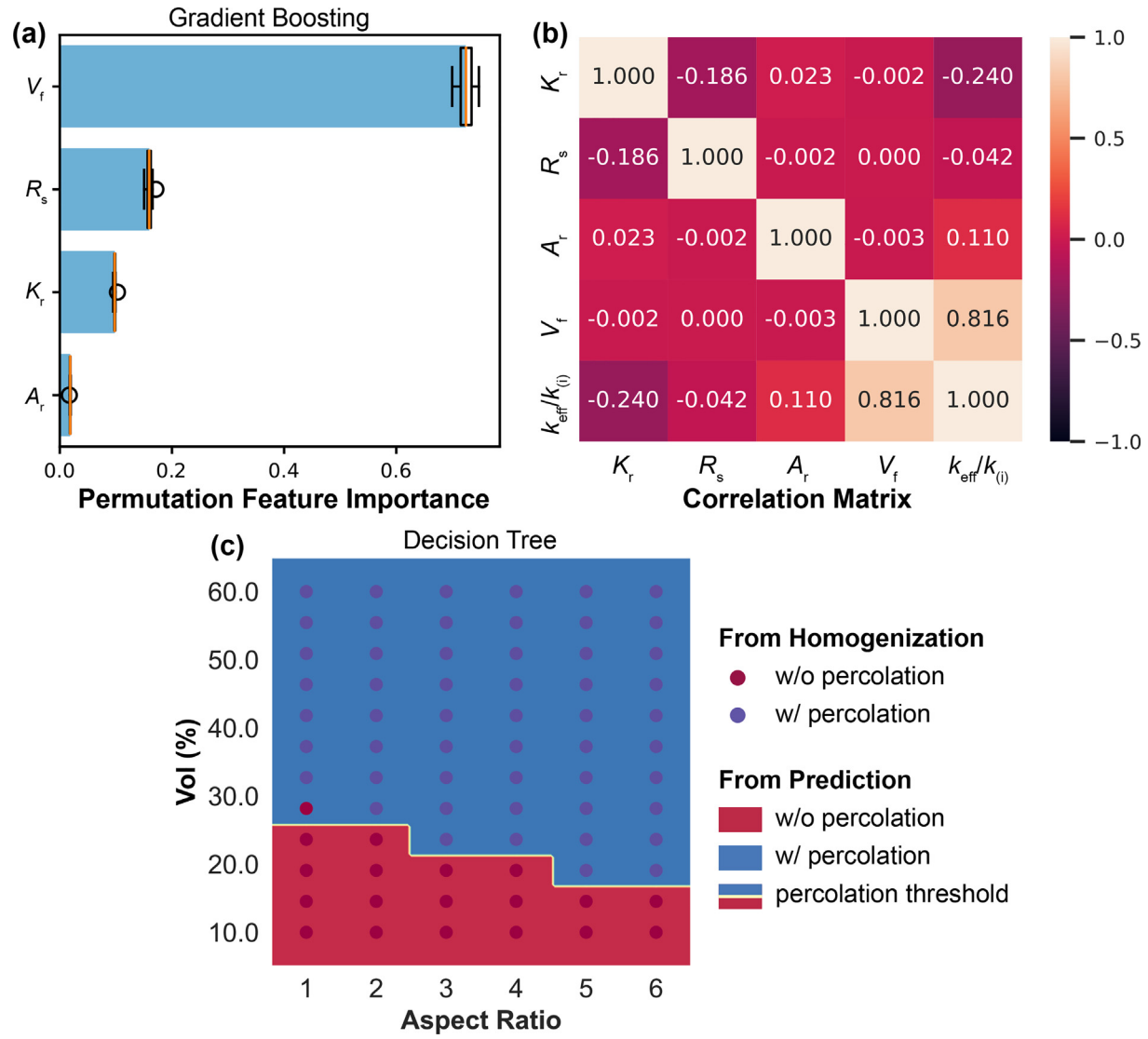

Fig. 9. SA results obtained through the (a) permutation importance and (b) Pearson coefficient methods; (c) classification of microstructures with the DT surrogate model.

path plays an important role in facilitating the heat flux in the material, and this percolation path is more likely to form in a system with higher V_f and A_r.

(ii)It was shown that in the microstructure in which particles have higher A_r, $\widetilde{R}_s$, and K_r, the percolation path plays an important role in facilitating heat flux in the material. In these cases, the percolated phases experience a high amount of internal thermal flux.

(iii)Based on the permutation importance method used in the sensitivity study, the particle volume fraction, followed by the interface thermal resistance, is the most influential parameter determining the effective thermal conductivity of the analyzed microstructure. An understanding of the importance of different parameters is particularly important for designing new material systems with desired properties. This shows that to control and optimize the effective thermal conductivity, not only the thermal conductivity of the filler but also the surface area of the fillers are important factors that should be tuned.

(iv)A surrogate-based classification model using the DT algorithm can successfully distinguish the RVEs with and without percolation paths by accessing information about the geometric parameters of the composites, i.e., A_r and V_f.

(v)A surrogate model based on the GB algorithm was developed to predict the effective thermal conductivity of the microstructures, which was much faster than numerical methods such as FEM simulations.

The proposed workflow supports the study of material systems with more than two phases and composite structures with irregular particle sizes and shapes as a future extension. Future work will focus on particle segmentation and automated feature extraction of experimental image data [50], along with the development of DL models that work directly with the images as input and can predict the properties of the representative structures of experimental images.

Data availability

The authors declare that the data supporting the findings of this study are available within the paper. Source codes of MOOSE-based application NIsoS and related utilities are cured in the online repository {bitbucket.org/mfm_tuda/nisos.git}. The simulation results, statistics and metadata are cured in the online dataset (DOI: 10.5281/zenodo.7043464).

Declaration of Competing Interest

The authors declare that they have no known competing financial interests or personal relationships that could have appeared to influence the work reported in this paper.

Acknowledgements

The authors acknowledge the financial support of the German Science Foundation (DFG) in the framework of the Research Training Groups 2561 (GRK 2561, project number 413956820, subprojects A4 and A6). The authors greatly appreciate the computing time granted by the NHR4CES Resource Allocation Board under the project "special00007", provided on the Lichtenberg II High-Performance Computer and the technique supported by the HHLR, Technische Universität Darmstadt. The authors also thank B. Lin for his help in conceptualizing the issues in the data-driven part and P. Kühn for his extensive revision of the manuscript regarding language and grammar.

References

[1] S. Zhai, P. Zhang, Y. Xian, J. Zeng, B. Shi, Effective thermal conductivity of polymer composites: Theoretical models and simulation models, Int. J. Heat Mass Transf. 117 (2018) 358–374.
[2] J.-P. Cao et al., Improved thermal conductivity and flame retardancy in polystyrene/poly(vinylidene fluoride) blends by controlling selective localization and surface modification of sic nanoparticles, ACS Appl. Mater. Interfaces 5 (2013) 6915–6924.
[3] Z. Han, A. Fina, Thermal conductivity of carbon nanotubes and their polymer nanocomposites: A review, Prog. Polym. Sci. 36 (2011) 914–944.
[4] M.R.P. Elenchezhian, V. Vadlamudi, R. Raihan, K. Reifsnider, Data driven composites: the challenge and paths forwards, in: Proceedings of CAMX 2018 Conference, Dallas, TX, 2018.
[5] D. Stauffer, A. Aharony, Introduction to percolation theory, Taylor & Francis, 2018.
[6] G. Zhang et al., A percolation model of thermal conductivity for filled polymer composites, J. Compos. Mater. 44 (2010) 963–970.
[7] I.Y. Forero-Sandoval et al., Electrical and thermal percolation in two-phase materials: A perspective, J. Appl. Phys. 131 (2022) 230901.
[8] A. Aryanfar et al., 3d percolation modeling for predicting the thermal conductivity of graphene-polymer composites, Comput. Mater. Sci. 197 (2021) 110650.
[9] F. Kargar et al., Thermal percolation threshold and thermal properties of composites with high loading of graphene and boron nitride fillers, ACS Appl. Mater. Interfaces 10 (2018) 37555–37565.
[10] W. Xu, P. Lan, Y. Jiang, D. Lei, H. Yang, Insights into excluded volume and percolation of soft interphase and conductivity of carbon fibrous composites with core-shell networks, Carbon 161 (2020) 392–402.
[11] W. Xu, M. Jia, Z. Gong, Thermal conductivity and tortuosity of porous composites considering percolation of porous network: From spherical to polyhedral pores, Compos. Sci. Technol. 167 (2018) 134–140.
[12] W. Xu, Y. Jiao, Theoretical framework for percolation threshold, tortuosity and transport properties of porous materials containing 3d non-spherical pores, Int. J. Eng. Sci. 134 (2019) 31–46.
[13] W. Xu, Y. Zhang, J. Jiang, Z. Liu, Y. Jiao, Thermal conductivity and elastic modulus of 3d porous/fractured media considering percolation, Int. J. Eng. Sci. 161 (2021) 103456.
[14] K.M. Shahil, A.A. Balandin, Thermal properties of graphene and multilayer graphene: Applications in thermal interface materials, Solid State Commun. 152 (2012) 1331–1340.
[15] R.A. Medina-Esquivel et al., Thermal characterization of composites made up of magnetically aligned carbonyl iron particles in a polyester resin matrix, J. Appl. Phys. 111 (2012) 054906.
[16] W. Tian, R. Yang, Phonon transport and thermal conductivity percolation in random nanoparticle composites, Tech Sci. Press CMES 24 (2008) 123–141.
[17] G. Amirthan, A. Udaya kumar, M. Balasubramanian, Thermal conductivity studies on si/sic ceramic composites, Ceram. Int. 37 (2011) 423–426.
[18] J.C. Maxwell, A treatise on electricity and magnetism, vol. 1, Clarendon press, 1873.
[19] V.D. Bruggeman, Berechnung verschiedener physikalischer konstanten von heterogenen substanzen. i. dielektrizitätskonstanten und leitfähigkeiten der mischkörper aus isotropen substanzen, Ann. Phys. 416 (1935) 636–664.
[20] X. Yang et al., Finite element prediction of the thermal conductivity of gnp/al composites, Acta Metall. Sin. (Engl. Lett.) 35 (2022) 825–838.
[21] A. Sharma, T. Mukhopadhyay, S.M. Rangappa, S. Siengchin, V. Kushvaha, Advances in computational intelligence of polymer composite materials: machine learning assisted modeling, analysis and design, Arch. Comput. Methods Eng. 1–45 (2022).
[22] G. Pilania, Machine learning in materials science: From explainable predictions to autonomous design, Comput. Mater. Sci. 193 (2021) 110360.
[23] H. Wei, S. Zhao, Q. Rong, H. Bao, Predicting the effective thermal conductivities of composite materials and porous media by machine learning methods, Int. J. Heat Mass Transf. 127 (2018) 908–916.
[24] L. Himanen, A. Geurts, A.S. Foster, P. Rinke, Data-driven materials science: status, challenges, and perspectives, Adv. Sci. 6 (2019) 1900808.
[25] E.A. Olivetti et al., Data-driven materials research enabled by natural language processing and information extraction, Appl. Phys. Rev. 7 (2020) 041317.
[26] H. Wei, H. Bao, X. Ruan, Machine learning prediction of thermal transport in porous media with physics-based descriptors, Int. J. Heat Mass Transf. 160 (2020) 120176.
[27] S. Schneeweiss, Sensitivity analysis and external adjustment for unmeasured confounders in epidemiologic database studies of therapeutics, Pharmacoepidemiol. Drug Saf. 15 (2006) 291–303.
[28] B. Liu, N. Vu-Bac, X. Zhuang, T. Rabczuk, Stochastic multiscale modeling of heat conductivity of polymeric clay nanocomposites, Mech. Mater. 142 (2020) 103280.
[29] B. Lin, Y. Bai, B.-X. Xu, Data-driven microstructure sensitivity study of fibrous paper materials, Mater. Des. 197 (2021) 109193.
[30] C.F. Matt, M.E. Cruz, Effective thermal conductivity of composite materials with 3-D microstructures and interfacial thermal resistance, Numer. Heat Transf. Part A Appl. 53 (2008) 577–604.
[31] A.M. Thiele, A. Kumar, G. Sant, L. Pilon, Effective thermal conductivity of three-component composites containing spherical capsules, Int. J. Heat Mass Transf. 73 (2014) 177–185.
[32] A. Javili, S. Kaessmair, P. Steinmann, General imperfect interfaces, Comput. Methods Appl. Mech. Eng. 275 (2014) 76–97.
[33] D. Marcos-Gómez, J. Ching-Lloyd, M.R. Elizalde, W.J. Clegg, J.M. Molina-Aldareguia, Predicting the thermal conductivity of composite materials with imperfect interfaces, Compos. Sci. Technol. 70 (2010) 2276–2283.
[34] J. Yvonnet, Q.-C. He, Q.-Z. Zhu, J.-F. Shao, A general and efficient computational procedure for modelling the kapitza thermal resistance based on xfem, Comput. Mater. Sci. 50 (2011) 1220–1224.
[35] J.T. Liu, S.T. Gu, E. Monteiro, Q.C. He, A versatile interface model for thermal conduction phenomena and its numerical implementation by XFEM, Comput. Mech. 53 (2014) 825–843.
[36] A. Aalilija, C.-A. Gandin, E. Hachem, A simple and efficient numerical model for thermal contact resistance based on diffuse interface immersed boundary method, Int. J. Therm. Sci. 166 (2021) 106817.
[37] Y. Yang et al., A diffuse-interface model of anisotropic interface thermal conductivity and its application in thermal homogenization of composites, Scr. Mater. 212 (2022) 114537.
[38] S.G. Kim, W.T. Kim, T. Suzuki, Phase-field model for binary alloys, Phys. Rev. E 60 (1999) 7186–7197.
[39] M.R. Tonks, D. Gaston, P.C. Millett, D. Andrs, P. Talbot, An object-oriented finite element framework for multiphysics phase field simulations, Comput. Mater. Sci. 51 (2012) 20–29.
[40] C.J. Permann et al., MOOSE: Enabling massively parallel multiphysics simulation, SoftwareX 11 (2020) 100430.
[41] F. Pedregosa et al., Scikit-learn: Machine learning in Python, J. Mach. Learn. Res. 12 (2011) 2825–2830.
[42] M. Gardner, S. Dorling, Artificial neural networks (the multilayer perceptron)—a review of applications in the atmospheric sciences, Atmos. Environ. 32 (1998) 2627–2636.
[43] N.K. Chauhan, K. Singh, A review on conventional machine learning vs deep learning, in: 2018 International Conference on Computing, Power and Communication Technologies, GUCON, 2018, pp. 347–352.
[44] I. Gitman, H. Askes, L. Sluys, Representative volume: Existence and size determination, Eng. Fract. Mech. 74 (2007) 2518–2534.
[45] R. Hill, Elastic properties of reinforced solids: some theoretical principles, J. Mech. Phys. Solids 11 (1963) 357–372.
[46] Z. Hashin, Analysis of composite materials—a survey, J. Appl. Mech. 50 (1983) 481–505.
[47] X. Lu et al., Numerical homogenization of thermal conductivity of particle-filled thermal interface material by fast fourier transform method, Nanotechnology 32 (2021) 265708.
[48] H.T. Kim, High thermal conductivity ceramics and their composites for thermal management of integrated electronic packaging, in: K. Volkov (Ed.), Heat Transfer, IntechOpen, Rijeka, 2018. Chapter 16.
[49] A. Decarlis, M. Jaeger, R. Martin, Determination of the effective thermal conductivity tensor of heterogeneous media using a self-consistent finite element method: Application to the pseudo-percolation thresholds of mixtures containing nonspherical inclusions, J. Heat Transf. 122 (1999) 171–175.
[50] B. Lin et al., A deep learned nanowire segmentation model using synthetic data augmentation, npj Comput. Mater. 8 (2022) 1–12.